Separation of static and dynamic sources in absence epileptic seizures using depth cortical measurements

Saeed Akhavan, Ronald Phlypo, Mahmoud Kamarei, Hamid Soltanian-Zadeh, Christian Jutten

Separation of Static and Dynamic Sources in Absence Epileptic Seizures Using Depth Cortical Measurements

S. AKHAVAN[a,b], R. PHLYPO[b], M. KAMAREI[a], H. SOLTANIAN-ZADEH[a,c], C. JUTTEN[b,d]

[a] *School of Electrical and Computer Engineering, University of Tehran, Tehran, Iran*
[b] *Univ. Grenoble Alpes, Grenoble INP, CNRS, GIPSA-lab, Grenoble, France*
[c] *Medical Image Analysis Lab., Henry Ford Health System, Detroit, MI, USA*
[d] *Institut Universitaire de France, Paris, France*

Abstract

In this study, we analyze the absence epileptic seizures using the data recorded from different layers of somatosensory cortex of absence epileptic rats. We aim to 1) extract the epileptic activities or sources generating the seizures, and 2) investigate the temporal changes of seizures. To achieve our goals, we describe the recorded seizures by a linear superposition of static and dynamic sources. The static sources are stable and have a fixed structure, while the dynamic sources can be intermittent, and may be with different locations. Retrieving the sources and their structures from the recorded seizures helps us to achieve the desired analysis. Experimental results show the existence of a static source and three specific dynamic sources during the recorded seizures. The dynamic sources randomly activate with the static source and one of them disappears towards the end of the seizures. Moreover, it is shown that the spatial locations of the sources are similar in different absence epileptic rats.

Keywords: Absence epilepsy; seizure; static sources; dynamic sources; static structure; dynamic structure

1. Introduction

Absence epilepsy is one of the several kinds of epilepsy which is more common in children [12, 6]. Sudden emergence of seizures associated with appearance of spike and wave discharges in electroencephalogram (EEG) recordings is the indication of absence epilepsy [32, 17].

Analysis of absence epileptic seizures has been a challenging problem over the past decades [5, 30, 4, 27]. For instance, [4] investigates the temporal changes of the brain activities during seizures using intracranial EEG data recorded from Genetic Absence Epilepsy Rat from Strasbourg (GAERS), which is one of the well-validated animal model for absence epilepsy [34]. At first, source separation methods are applied on temporal sliding windows of the data, and the

relevant temporal sources are estimated for each window. Then, by comparing the sources in different time windows, it is shown that they become more stationary after a latency from the onset of seizures.

The analysis of absence epileptic seizures has also been done in humans [31, 42, 30]. For instance in [31], the EEG-fMRI data were acquired from 13 patients suffering from absence epilepsy. Then, by applying gamma function regressors on sliding time windows of the data, and calculating the F-value, it was shown that the cortical activations and deactivations tend to occur earlier than the thalamic responses during seizures. As another example in [42], neuromagnetic sources were volumetrically scanned with accumulated source imaging from 14 patients. Then, effective connectivity networks of the entire brain, including the cortico–thalamo network, were evaluated at the source level through Granger causality analysis [37]. The obtained results show that the cortico–thalamic effective connectivity increases during seizures. Moreover, the direction of the connectivity is predominantly from the cortex to the thalamus in the beginning of seizures.

Neuroscientists investigated a lot the networks involved in seizures and the spatial localization of their starting points [33, 41]. Several theories have been suggested about the spatial localization of seizures. Some of them point to cortex as the main origin, while a few of them consider thalamus area as the main origin of seizures [8]. The most recent theory filling the gap between cortical and thalamic origin is that both cortex and thalamus participate in the generation of seizures [29, 39]. By investigating the non-linear correlations between the recorded signals from cortex and thalamus in the Wistar Absence Glaxo from Rijswik (WAG/Rij) rat model, it has been shown that in the beginning of seizures, somatosensory cortex drives thalamus, while thereafter, somatosensory cortex and thalamus drive each other until the end of seizures [29]. Existence of a cortical starting area has also been recognized in GAERS [34].

A second step is now to wonder if one can define a more accurate localization of epileptic events, by studying what happens in the different layers of the somatosensory cortex. In this purpose, a data set was acquired in Grenoble Institute of Neurosciences (GIN) from different layers of somatosensory cortex of GAERS. In this study, we explore the seizures using the recorded data. We aim to answer the following questions:

1) Which epileptic activities or sources generate the recorded seizures?

2) How do the recorded seizures change over time?

It must be mentioned that all previous researches have investigated the seizures using the data recorded from different areas of the brain, however, this is the first study that explores the seizures using the data recorded from one "column" of the cortex. The data were recorded using a set of very close sensors (leads) distributed along a needle located in somatosensory cortex. Hence, they were acquired from different layers of a cortex "column". We describe the recorded seizures by a linear combination of epileptic sources. We assume that there are two kinds of sources during seizures, static and dynamic sources. Static sources model the background epileptic activities and dynamic sources are complementary to static sources in the modelization of spikes, which are the

typical shapes during a seizure. The static sources are stable and have a fixed structure with respect to the recording electrode, while the dynamic sources are intermittent and their positions may change along the seizure. We propose a method to retrieve the static and dynamic sources and their structures from the recorded seizures. Then, we analyze the recorded seizures and answer the mentioned questions using the obtained results.

The initial idea of this study was published in the conference article [1]. In this study, we present a comprehensive treatment of the initial idea including 1) the explanation of the data acquisition and the necessary preprocessing steps, 2) the accurate definition of the considered model with its physiological and mathematical reasons, 3) the explanation of the proposed method with all of its important mathematical details, 4) the verification of the proposed method using simulations, and 5) the interpretation and cross-validation of the results obtained from the neural data set.

The rest of the paper is organized as follows. Section 2 introduces the characteristics of the data and the considered model for seizures. Problem formulation and considered assumptions are stated in Section 3. The proposed method for estimating the model parameters is explained in Section 4, while Section 5 is dedicated to simulations and experimental results. Finally, the discussion and concluding remarks are reported in Section 6.

2. Materials

2.1. Data

The dataset used in this study was recorded from the somatosensory cortex of four adult GAERS. One electrode with sixteen sensors ($n = 16$) with an inter-distance of $150\,\mu$m was perpendicularly inserted in the somatosensory cortex (Fig. 1), so that the different sensors measured the extracellular field potentials in different layers of somatosensory cortex [20, 28]. The recording region was accurately determined by neuroscientists before the data acquisition. The sampling frequency was $f_s = 20\,$kHz. More details about the data acquisition process can be found in [18]. All the experiments were submitted and approved by the local Ethical Committee and European Union guidelines (directive 86/609/EEC).

Appearance of spikes in seizures is the most important indication of absence epilepsy. In the recorded data, the spikes appear in different channels simultaneously during the seizures because the data has been acquired very locally. Hence, we can consider each $n = 16$ spikes (at the same time) as one time window, and consider each seizure as a train of spike time windows as shown in Fig. 1.

2.2. Model for Seizures

In our work regarding spatio-temporal modeling of absence seizures [2], we assumed hidden states during a seizure. Each spike of a seizure is produced when one of the hidden states is activated. We also assumed that each state has a

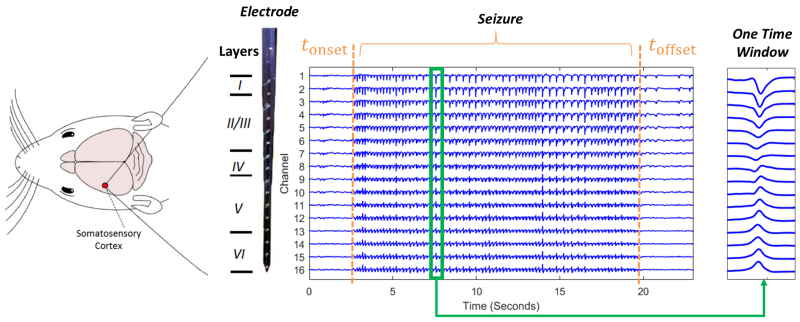

Figure 1: From left to right, implementation scheme, recording electrode, a seizure and a time window (length of 87.5 ms) Each time window represents a spike recorded on a electrode constituted of $n = 16$ sensors, and shows the recorded signals in different layers of the cortex. The seizure onset and the end of the seizure are indicated by t_{onset} and t_{offset}, respectively.

few specific substates, which generate the spike in that state. By extracting the states and their substates, we showed that there were some specific substates which were common in all of the states. Hence, they always participated in the generation of spikes during the seizures. In other words, there were some background activities during the seizures. Based on these results, we consider the following static-dynamic model in this study.

We assume that some physical activities or phenomena are taking place during the seizures and the sensors on the electrode record the instantaneous linear combination of the signals produced by the mentioned sources. Since somatosensory cortex is the main onset region of seizures, we assume that the sources are located in the vicinity of the recording electrode. The mixture of the signals is considered linear and instantaneous due to the quasi-static assumption of Maxwell's laws. We assume that there are two kinds of sources during the seizures, static and dynamic sources.

Static Sources: The position of the static sources is fixed. The static sources always participate in the generation of the seizures. The static sources statistically can be non-stationary. For instance, their amplitude may change in different time windows, however, they are always on and contribute in the generation of the data. The contribution of the static sources in the generation of the data is shown by a matrix called the static structure. The number of static sources is fixed and equal to m ($m < n$).

Dynamic Sources: Unlike static sources, a dynamic source sometimes participates in the generation of the data, and it may be off in some of the time windows. The location of dynamic sources may change in different layers of somatosensory cortex over time. In each time window, the contribution of the dynamic sources in the generation of the data is shown by a matrix called the dynamic structure. The number of dynamic sources in each time window is unknown.

Schematic diagrams of the considered model for three time windows are

shown in Fig. 2. All of the sources and their structures in different time windows are unknown and we should retrieve them from the recorded seizures. In the following, we explain how the time windows are considered for a seizure.

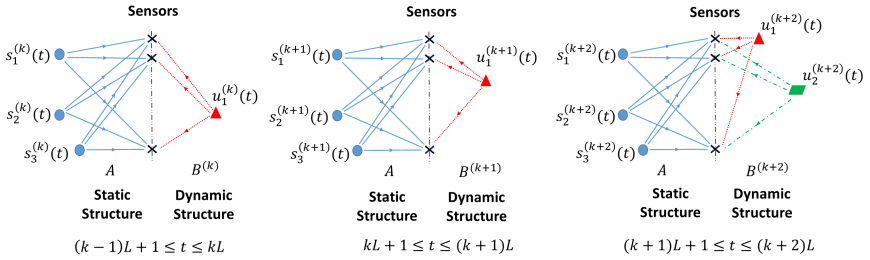

Figure 2: Static and dynamic sources for three consecutive time windows. The static sources ($\mathbf{s}_1$, $\mathbf{s}_2$, $\mathbf{s}_3$) and the dynamic sources ($\mathbf{u}_1$, $\mathbf{u}_2$) are shown in the left and right sides of the sensors, respectively. The position of the static sources with respect to the sensors is fixed, while the position of the dynamic sources change.

2.3. Time Windows of Seizures

As mentioned in subsection 2.1, we consider each $n = 16$ spikes (at the same time) as one time window as shown in Fig. 1. For this purpose, we must at first separate the seizures from the data, and then, detect the spikes during the seizures.

Since the amplitude of the signals changes significantly at the beginning and at the end of the seizures, we separate the seizures from the data by simple thresholding. Since the data are intracranial recordings and they are not too noisy, we employ the thresholding method for separating the seizures from the data. However, if the data were noisy such as scalp EEG recordings, more efficient methods such as proposed in [25] are required for separating the seizures from the data. A good survey on seizure detection methods can be found in [3]. It is also worth mentioning that the focus of this study is on analyzing the seizures, however, the data between seizures are also valuable. These data can be processed to predict the occurrence of seizures. For instance, authors of [24] analyzed the data between seizures using a well-known criterion called permutation entropy, and achieved the average anticipation time around 4.9 s. The data analyzed in [24] were EEG data acquired from GAERS rats.

Once the seizures are separated from the data, we individually detect the spikes for each seizure following the proposed method in [35] and construct the time windows (each of length 87.5 ms, $L = 1750$ samples). We also align the time windows using the improved version of Woody's method proposed in [10] to achieve higher correlation among the time windows, and get accurate results. Finally, the time windows are consecutively placed for each seizure separately. Thus, a seizure constituted by K spikes, is represented by the concatenation of its K elementary time windows. Hence, we remove the part of the recordings, which are not directly related to spikes. Now, we define our problem on the time windows of a seizure for estimating the model parameters.

3. Problem statement

3.1. Problem Formulation

Assume that the considered seizure has K elementary time windows, and each time window consists of L samples. For the k^{th} time window, we express the data at each time instant t as follows:

$$\mathbf{y}^{(k)}(t) = \mathbf{A}\mathbf{s}^{(k)}(t) + \mathbf{B}^{(k)}\mathbf{u}^{(k)}(t) + \mathbf{n}^{(k)}(t) \qquad t = 1, 2, ..., L \tag{1}$$

where $\mathbf{y}_t^{(k)} = [y_1^{(k)}(t), ..., y_n^{(k)}(t)]^T \in \mathbb{R}^n$, $\mathbf{A} \in \mathbb{R}^{n \times m}$ and $\mathbf{s}_t^{(k)} = [s_1^{(k)}(t), ..., s_m^{(k)}(t)]^T \in \mathbb{R}^m$ represent the recorded signals on the sensors, the static structure and the static sources, respectively. If we assume that the total number of dynamic sources activated in the k^{th} time window is equal to r_k, $\mathbf{B}^{(k)} \in \mathbb{R}^{n \times r_k}$ and $\mathbf{u}_t^{(k)} = [u_1^{(k)}(t), ..., u_{r_k}^{(k)}(t)]^T \in \mathbb{R}^{r_k}$ show the dynamic structure and the dynamic sources, respectively. It should be noted that $\mathbf{A}$ is common to all time windows, while $\mathbf{B}^{(k)}$ is changing on each time window. Finally, $\mathbf{n}_t^{(k)} = [n_1^{(k)}(t), ..., n_n^{(k)}(t)]^T \in \mathbb{R}^n$ is an independent and identically distributed (i.i.d.) noise vector at different sensors, which is considered to be a zero-mean Gaussian noise with an unknown covariance matrix $\mathbf{\Sigma}_N \in \mathbb{R}^{n \times n}$.

For each time window k ($k = 1, 2, ..., K$), if we concatenate the L vectors (samples) of the recorded signals, the static sources, the dynamic sources and the noise, we obtain the matrices $\mathbf{Y}^{(k)} \in \mathbb{R}^{n \times L}$, $\mathbf{S}^{(k)} \in \mathbb{R}^{m \times L}$, $\mathbf{U}^{(k)} \in \mathbb{R}^{r_k \times L}$ and $\mathbf{N}^{(k)} \in \mathbb{R}^{n \times L}$. Therefore, (1) can be written as:

$$\mathbf{Y}^{(k)} = \mathbf{A}\mathbf{S}^{(k)} + \mathbf{B}^{(k)}\mathbf{U}^{(k)} + \mathbf{N}^{(k)} \tag{2}$$

Hence, the set of unknown parameters (Θ) can be expressed as

$$\Theta = \{\mathbf{A}, \bigcup_{k=1}^{K} \{\mathbf{S}^{(k)}, r_k, \mathbf{B}^{(k)}, \mathbf{U}^{(k)}\}\} \tag{3}$$

We aim to extract Θ using recorded signals in all of the time windows, i.e., $\mathbf{Y}^{(k)}$ for $k = 1, 2, ..., K$.

3.2. Known Characteristics of The System

The following assumptions are considered in the procedure of parameters extraction.

($\mathcal{A}1$) The number of static sources (m) is a constant for all the seizures, and it is determined by physiological reasons.

Neuroscientists have spatially and temporally explored the spike and wave discharges generating the seizures, and they have shown that these spike and wave discharges are similar in different seizures of a specific rat [18, 29, 34]. In other words, there is intra-rat similarity between the seizures. We use this suitable physiological information to obtain m. In fact, we expect to obtain results with intra-rat similarity. For this purpose, we extract the model parameters by

considering different m. Then, the number of static sources which leads to the results with better intra-rat similarity is considered as the optimum number of static sources. It is worth mentioning that the similarity between results can be measured by the cross correlation coefficient.

($\mathcal{A}2$) The total number of static and dynamic sources ($m + r_k$) is less than the number of sensors (n) in each time window.

Consider (2) without presence of noise:

$$\mathbf{Y}^{(k)} = [\mathbf{A} \;\; \mathbf{B}^{(k)}] \begin{bmatrix} \mathbf{S}^{(k)} \\ \mathbf{U}^{(k)} \end{bmatrix} \tag{4}$$

If we assume $[\mathbf{A} \;\; \mathbf{B}^{(k)}] \in \mathbb{R}^{n \times (m+r_k)}$ is known, it is needed to compute the inverse of $[\mathbf{A} \;\; \mathbf{B}^{(k)}]$ for estimating the sources. Therefore, $m + r_k \leq n$ and $[\mathbf{A} \;\; \mathbf{B}^{(k)}]$ must be a full column rank matrix.

($\mathcal{A}3$) The columns of $\mathbf{A}$ are unit norm.

To omit the scaling ambiguity problem in separation of the static sources, the columns of $\mathbf{A}$ are considered unit norm vectors [15].

($\mathcal{A}4$) Static sources and dynamic sources are considered uncorrelated in each time window.

When the sources are considered uncorrelated, it means that there is no linear synchronization between them. Mathematically, we can write:

$$\begin{aligned} &\frac{1}{L}\sum_{t=1}^{L} \mathbf{s}^{(k)}(t)\mathbf{u}^{(k)}(t)^T = \mathbf{0} \in \mathbb{R}^{m \times r_k} \\ &\frac{1}{L}\sum_{t=1}^{L} \mathbf{s}^{(k)}(t)\mathbf{s}^{(k)}(t)^T = \mathbf{\Lambda}_s^{(k)} \in \mathbb{R}^{m \times m} \\ &\frac{1}{L}\sum_{t=1}^{L} \mathbf{u}^{(k)}(t)\mathbf{u}^{(k)}(t)^T = \mathbf{\Lambda}_u^{(k)} = \mathbf{I} \in \mathbb{R}^{r_k \times r_k} \end{aligned} \tag{5}$$

where $\Lambda_s^{(k)}$ is the auto-correlation matrix of the static sources in the k^{th} time window and unknown. It is a diagonal matrix with positive entries which are not necessarily constant during different time windows. Auto-correlation matrix of dynamic sources ($\Lambda_u^{(k)}$) is considered equal to identity matrix ($\mathbf{I}$) in order to omit the scaling ambiguity problem in separation of dynamic sources [15].

($\mathcal{A}5$) The dynamic sources are considered statistically independent in each time window.

There is no synchronization between the dynamic sources, and they may randomly activate in each time window. Hence, we assume that they are statistically independent. It should be noted that two random variables (X, Y) are independent when their joint probability distribution is the product of their marginal probability distributions, i.e.,

$$p_{X,Y}(x, y) = p_X(x)\, p_Y(y) \tag{6}$$

If X and Y are independent, then, they are also uncorrelated because

$$E_{X,Y}(xy) = E_X(x)\, E_Y(y) \tag{7}$$

However, the reverse of this remark is not correct. This means that if X and Y are uncorrelated, then they are not essentially independent. Hence, independency is a stronger condition than uncorrelatedness [15].

($\mathcal{A}6$) The noise is uncorrelated with all of the sources in each time window.

Since the noise is zero-mean and independent of the sources, it is uncorrelated with all of the sources in each time window, i.e.,

$$\begin{aligned} \frac{1}{L}\sum_{t=1}^{L} \mathbf{s}^{(k)}(t)\mathbf{n}^{(k)}(t)^T &= \mathbf{0} \in \mathbb{R}^{m\times n} \\ \frac{1}{L}\sum_{t=1}^{L} \mathbf{u}^{(k)}(t)\mathbf{n}^{(k)}(t)^T &= \mathbf{0} \in \mathbb{R}^{r_k\times n} \end{aligned} \tag{8}$$

Now, the problem statement is complete. The goal is estimating the set of unknown parameters (Θ) from the time windows of a recorded seizure ($\mathbf{Y}^{(k)}$ for $k = 1, 2, ..., K$) based on the known characteristics of the model.

4. Proposed Method

At first, we estimate the static structure ($\mathbf{A}$) and the number of dynamic sources in each time window (r_k). Then, the dynamic sources ($\mathbf{U}^{(k)}$) are obtained in each time window. Finally, we estimate the static sources ($\mathbf{S}^{(k)}$) and the dynamic structure ($\mathbf{B}^{(k)}$) in each time window.

4.1. Extraction of The Static Structure and The Number of Dynamic Sources

We follow the proposed method in [44], regarding the joint diagonalization of a set of target matrices, to estimate the static structure and the number of dynamic sources in each time window. Since the sources are uncorrelated according to ($\mathcal{A}4$), we solve the following optimization problem:

$$\begin{aligned} \widehat{\Theta}_1 &= \underset{\Theta_1}{\operatorname{argmin}}\ \ g(\Theta_1) \\ \Theta_1 &= \{\mathbf{A},\ \bigcup_{k=1}^{K} \{\, \mathbf{\Lambda}_s^{(k)},\, r_k\, , \mathbf{R}_B^{(k)}\}\} \\ g(\Theta_1) &= \sum_{k=1}^{K} \|\mathbf{R}_y^{(k)} - \mathbf{A}\mathbf{\Lambda}_s^{(k)}\mathbf{A}^T - \underbrace{\mathbf{B}^{(k)}\overbrace{\mathbf{\Lambda}_u^{(k)}}^{\mathbf{I}}\mathbf{B}^{(k)^T}}_{\mathbf{R}_B^{(k)}}\|_F^2 \end{aligned} \tag{9}$$

where $\mathbf{R}_B^{(k)} = \mathbf{B}^{(k)}\mathbf{\Lambda}_u^{(k)}\mathbf{B}^{(k)^T}$, $\|.\|_F$ denotes the Frobenius norm, and the autocorrelation matrix of the recorded signals ($\mathbf{R}_y^{(k)} \in \mathbb{R}^{n\times n}$) in the k^{th} time window

is calculated as follows:

$$\mathbf{R}_y^{(k)} = \frac{1}{L}\sum_{t=1}^{L}\mathbf{y}^{(k)}(t)\mathbf{y}^{(k)}(t)^T \tag{10}$$

It should be mentioned that $\mathbf{\Lambda}_s^{(k)}$ is not an important parameter, but it must be estimated during the optimization. The other noticeable point is that the rank of $\mathbf{R}_B^{(k)}$ is equal to r_k, and since $r_k < n$, it is a low-rank matrix. We use this information to extract the number of dynamic sources (r_k) in each time window.

The following constraints must also be considered in the optimization:

c_1) The columns of $\mathbf{A}$ are unit norms.

c_2) $\mathbf{\Lambda}_s^{(k)}$ is diagonal with positive entries.

c_3) $\mathbf{R}_B^{(k)}$ is a low-rank and positive semidefinite matrix ($\mathbf{R}_B^{(k)} \succeq 0$).

We use alternating least square (ALS) method to solve the optimization problem. We consider some feasible initial values for Θ_1, then, we alternately perform the following steps until the convergence of the parameters.

Step 1. Assuming $\mathbf{\Lambda}_s^{(k)}$ and $\mathbf{R}_B^{(k)}$ for $k = 1, 2, ..., K$ are fixed, we have:

$$\begin{aligned}\widehat{\mathbf{A}} = \underset{\mathbf{A}}{\operatorname{argmin}} &\sum_{k=1}^{K}\|\mathbf{R}_y^{(k)} - \mathbf{A}\mathbf{\Lambda}_s^{(k)}\mathbf{A}^T - \mathbf{R}_B^{(k)}\|_F^2 \\ s.t. \quad &\operatorname{diag}(\mathbf{A}^T\mathbf{A}) = \mathbf{I}\end{aligned} \tag{11}$$

where $\operatorname{diag}(\mathbf{X})$ keeps the diagonal entries of $\mathbf{X}$, and makes the other entries equal to zero. This constrained optimization problem can easily be solved using gradient-projection (GP) method [22] (see Appendix A).

Step 2. Assuming $\mathbf{A}$ and $\mathbf{R}_B^{(k)}$ are fixed, we have:

$$\begin{aligned}\widehat{\mathbf{\Lambda}}_s^{(k)} = \underset{\mathbf{\Lambda}_s^{(k)}}{\operatorname{argmin}} &\|\mathbf{R}_y^{(k)} - \mathbf{A}\mathbf{\Lambda}_s^{(k)}\mathbf{A}^T - \mathbf{R}_B^{(k)}\|_F^2 \\ s.t. \quad &\mathbf{\Lambda}_s^{(k)} = \operatorname{diag}(\mathbf{\Lambda}_s^{(k)}), \quad \mathbf{\Lambda}_s^{(k)} \succeq 0\end{aligned} \tag{12}$$

This optimization problem is solved using non-negative least square (NNLS) method if we consider the vectorization form of all matrices in the problem (see Appendix B). This step must be performed for all of the time windows ($k = 1, 2, ..., K$) separately.

Step 3. Assuming $\mathbf{A}$ and $\mathbf{\Lambda}_s^{(k)}$ are fixed, we have:

$$\begin{aligned}\widehat{\mathbf{R}}_B^{(k)} = \underset{\mathbf{R}_B^{(k)}}{\operatorname{argmin}} &\|\mathbf{R}_y^{(k)} - \mathbf{A}\mathbf{\Lambda}_s^{(k)}\mathbf{A}^T - \mathbf{R}_B^{(k)}\|_F \\ s.t. \quad &\mathbf{R}_B^{(k)} \succeq 0, \quad \mathbf{R}_B^{(k)} \text{ is low-rank.}\end{aligned} \tag{13}$$

This step must also be performed for all of the time windows ($k = 1, 2, ..., K$) separately. We will explain later why we remove the power two in the objective

function. Since we must impose $\mathbf{R}_B^{(k)}$ to be a low-rank matrix, we use the penalty parameter to minimize both the objective function and the rank of $\mathbf{R}_B^{(k)}$. Hence, we have:

$$\widehat{\mathbf{R}}_B^{(k)} = \underset{\mathbf{R}_B^{(k)}}{\operatorname{argmin}} \|\mathbf{R}_y^{(k)} - \mathbf{A}\boldsymbol{\Lambda}_s^{(k)}\mathbf{A}^T - \mathbf{R}_B^{(k)}\|_F + \lambda^{(k)} \operatorname{rank}(\mathbf{R}_B^{(k)})$$
$$s.t. \quad \mathbf{R}_B^{(k)} \succeq 0 \tag{14}$$

where $\lambda^{(k)}$ is a penalty parameter which helps to minimize the rank of $\mathbf{R}_B^{(k)}$. Since minimization of rank function is an NP-hard problem [36], we approximate $\operatorname{rank}(\mathbf{R}_B^{(k)})$ with $\operatorname{Tr}\{\mathbf{R}_B^{(k)}\}$ which is a well-known convex relaxation for this function [11, 26]. The obtained optimization problem is very similar to the square root LASSO problem [9, 23], and it can be converted to a semidefinite programming (SDP) as shown in Appendix C. The main advantage of the square-root LASSO is that the penalty parameter can be obtained independently from variance of the noise. This is the main reason that we dropped the power of two in the objective function considered in (13). The final optimization problem can be solved using well known solvers like sdpt3 and cvx [40].

We repeat **Step 1**, **Step 2**, and **Step 3** until convergence, i.e., the parameters do not significantly change. Hence, the static structure ($\widehat{\mathbf{A}}$), the autocorrelation matrix of static sources ($\widehat{\boldsymbol{\Lambda}}_s^{(k)}$) and $\widehat{\mathbf{R}}_B^{(k)}$ for $k = 1, 2, ..., K$ are estimated. Finally, the number of dynamic sources in each time window is obtained as follows:

$$\widehat{r}_k = \operatorname{rank}(\widehat{\mathbf{R}}_B^{(k)}) \tag{15}$$

4.2. Extraction of Dynamic Sources

Consider the singular value decomposition (SVD) of the static structure as follows:

$$\mathbf{A} = \mathbf{V}\,\Sigma\,\mathbf{Q}^T, \qquad \mathbf{V} = [\underbrace{\mathbf{v}_1 \dots \mathbf{v}_m}_{\mathbf{V}_1}\ \underbrace{\mathbf{v}_{m+1} \dots \mathbf{v}_n}_{\mathbf{V}_2}] \tag{16}$$

where $\mathbf{V}_1 \in \mathbb{R}^{n\times m}$ is an orthonormal basis for the columns of $\mathbf{A}$ and $\mathbf{V}_2 \in \mathbb{R}^{n\times(n-m)}$ spans the null space of $\mathbf{A}$ because we know that $\operatorname{rank}(\mathbf{A}) = m$. Hence, if we left multiply both sides of (2) by $\mathbf{V}_2^T$, we can omit the contribution of the static sources in each time window:

$$\underbrace{\mathbf{V}_2^T\mathbf{Y}^{(k)}}_{\mathbf{Y}'^{(k)}} = \underbrace{\mathbf{V}_2^T\mathbf{A}\mathbf{S}^{(k)}}_{0} + \underbrace{\mathbf{V}_2^T\mathbf{B}^{(k)}}_{\mathbf{B}'^{(k)}}\mathbf{U}^{(k)} + \underbrace{\mathbf{V}_2^T\mathbf{N}^{(k)}}_{\mathbf{N}'^{(k)}} \tag{17}$$

where $\mathbf{Y}'^{(k)} \in \mathbb{R}^{(n-m)\times L}$, $\mathbf{B}'^{(k)} \in \mathbb{R}^{(n-m)\times r_k}$ and $\mathbf{N}'^{(k)} \in \mathbb{R}^{(n-m)\times L}$ are respectively the projected data, the projected dynamic structure and the projected noise in the k^{th} time window. The distribution of each column of the projected noise is $\mathcal{N}(\mathbf{0}, \mathbf{V}_2^T\boldsymbol{\Sigma}_N\mathbf{V}_2)$. The important point here is that we must be sure that $\mathbf{B}'^{(k)}$ is not equal to zero because the dynamic sources must be kept. According

to ($\mathcal{A}2$), since we assumed that $[\mathbf{A}\ \mathbf{B}^{(k)}] \in \mathbb{R}^{n\times(m+r_k)}$ is a full rank matrix, each column of $\mathbf{B}^{(k)}$ certainly exists in the space of $\mathbf{V}_2$, and hence, $\mathbf{B}'^{(k)}$ would not be equal to zero. Now, we can extract the dynamic sources in each time window.

According to ($\mathcal{A}5$), since we assumed that the dynamic sources are statistically independent, we are faced with an overdetermined BSS problem in the presence of noise. Hence, independent component analysis (ICA) can be applied to extract the dynamic sources ($\mathbf{U}^{(k)}$) from noisy measurements [7]. We use JADE algorithm to extract the dynamic sources [13]. Since we have estimated the number of dynamic sources (r_k) in the previous part, the dimension of the separating matrix $\mathbf{W}^{(k)} \in \mathbb{R}^{r_k\times(n-m)}$ is known, and regarding (17), we get:

$$\mathbf{W}^{(k)}\mathbf{Y}'^{(k)} = \mathbf{W}^{(k)}\mathbf{B}'^{(k)}\mathbf{U}^{(k)} + \mathbf{W}^{(k)}\mathbf{N}'^{(k)} \tag{18}$$

In fact, ICA tries to make the rows of $\mathbf{W}^{(k)}\mathbf{Y}'^{(k)}$ as much independent as possible. After applying ICA, the dynamic sources ($\widehat{\mathbf{U}}^{(k)}$) are determined.

For each time window, the explained procedure must be applied to retrieve the dynamic sources in all of the time windows.

4.3. Extraction of Static Sources and Dynamic Structure

When the static structure ($\mathbf{A}$) and the dynamic sources ($\mathbf{U}^{(k)}$) are determined, we can extract the static sources ($\mathbf{S}^{(k)}$) and the dynamic structure ($\mathbf{B}^{(k)}$) in each time window using the maximum log-likelihood estimator (MLE). It can be shown that minimizing the following objective function leads to finding the MLE solution of the parameters:

$$q(\mathbf{S}^{(k)}, \mathbf{B}^{(k)}) = \|\mathbf{Y}^{(k)} - \mathbf{A}\mathbf{S}^{(k)} - \mathbf{B}^{(k)}\mathbf{U}^{(k)}\|_F^2 \tag{19}$$

This objective function can simply be minimized using alternation minimization. For each time window, (19) must be minimized to retrieve the static sources ($\widehat{\mathbf{S}}^{(k)}$) and the dynamic structure ($\widehat{\mathbf{B}}^{(k)}$) in all of the time windows.

By determination of the static sources and the dynamic structure in all of the time windows, all parameters of the model are determined.

5. Simulation and Experimental Results

In this section, we first show the efficiency of the proposed method using simulated data. Then, the results obtained from depth recordings are presented.

5.1. Simulations

5.1.1. Data Generation

We generate the data according to (1) for each time window. The simulated data are different from the neural data, but we aim to provide simple signals with the same assumptions as the spikes in seizures, and check the efficiency of the different steps of the proposed method. We consider $K = 50$ time windows (each of length $L = 100$), $n = 10$ sensors, $m = 5$ static sources, and at most

$n - m = 5$ dynamic sources in each time window. The number of dynamic sources (r_k) is chosen randomly between 1 and 5 in each time window. Then, we generate the static structure $\mathbf{A}$ by a random matrix of size 10×5 with zero-mean and unit-variance i.i.d. Gaussian entries followed by normalizing the columns. In each time window, the static sources are considered as a mixture of three sine signals with different frequencies as follows:

$$s_i^{(k)}(t) = \sum_{j=1}^{3} \alpha_{ikj} \sin(2\pi(10i + 3j - 10) f_0\, t)$$
$$i = 1, 2, ..., 5, \qquad k = 1, 2, ..., 50,$$
$$1 \le t \le 100 \tag{20}$$

where $f_0 = \frac{1}{L} = 0.01$. The amplitude of sine signals (α_{ikj}) is uniformly distributed between 0 and 1. The static sources are not stationary because the amplitudes α_{ikj} change in different time windows, and according to ($\mathcal{A}4$), they are uncorrelated with each other because they have different frequencies in each time window. The entries of the dynamic structure in each time window $\mathbf{B}^{(k)} \in \mathbb{R}^{10 \times r_k}$ are independently chosen from zero-mean and unit-variance Gaussian distribution. The dynamic sources in each time window are again considered sine signals as follows:

$$u_i^{(k)}(t) = \sqrt{\frac{2L}{3}} \sum_{j=1}^{3} \sin(2\pi(10i + 3j + 40) f_0\, t)$$
$$i = 1, ..., r_k, \qquad k = 1, 2, ..., 50,$$
$$1 \le t \le 100 \tag{21}$$

where $\sqrt{\frac{2L}{3}}$ is equal to $\sqrt{\frac{200}{3}}$ in order to have unit norm dynamic sources. According to ($\mathcal{A}4$) and ($\mathcal{A}5$), the frequencies are selected such that the dynamic sources are mutually independent and uncorrelated with the static sources. Finally, each column of the noise $\mathbf{N}^{(k)}$ is generated from Gaussian distribution with zero-mean and covariance matrix $\sigma_0^2 \mathbf{I} \in \mathbb{R}^{10 \times 10}$ for all of the time windows. We also use the following criteria to evaluate the performance of the proposed method in estimation of the parameters:

$$Er_S = \underset{k}{\text{mean}} \frac{\|\mathbf{S}^{(k)} - \widehat{\mathbf{S}}^{(k)}\|_F^2}{\|\mathbf{S}^{(k)}\|_F^2}, \quad Er_A = \frac{\|\mathbf{A} - \widehat{\mathbf{A}}\|_F^2}{\|\mathbf{A}\|_F^2}, \quad Er_r = \underset{k}{\text{mean}} \frac{|r_k - \widehat{r}_k|}{r_k}$$
$$\text{Er}_U = \underset{k:\, r_k = \widehat{r}_k}{\text{mean}} \frac{\|\mathbf{U}^{(k)} - \widehat{\mathbf{U}}^{(k)}\|_F^2}{\|\mathbf{U}^{(k)}\|_F^2}, \quad Er_B = \underset{k:\, r_k = \widehat{r}_k}{\text{mean}} \frac{\|\mathbf{B}^{(k)} - \widehat{\mathbf{B}}^{(k)}\|_F^2}{\|\mathbf{B}^{(k)}\|_F^2} \tag{22}$$

where $\widehat{X}$ means estimated X. It should be noted that Er_r is not squared. We also consider the signal to noise (SNR) ratio as follows for the simulations:

$$\text{SNR} = 10\ \log(\frac{1}{K} \sum_{k=1}^{K} \frac{\|\mathbf{Y}^{(k)} - \mathbf{N}^{(k)}\|_F^2}{\|\mathbf{N}^{(k)}\|_F^2}) \tag{23}$$

5.1.2. Results

It is worth noting that we assume that the number of static sources ($m = 5$) is known during the simulations.

First Simulation: In this simulation, we consider σ_0^2 such that SNR $= 20\,dB$. The values of the criteria introduced in (22) are reported in the fifth row of Table 1. Moreover, the actual and estimated number of dynamic sources in each time window are shown in Fig. 3.

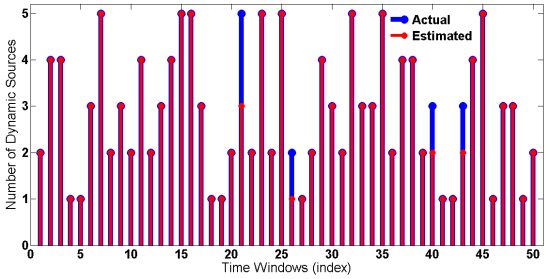

Figure 3: The actual and estimated number of dynamic sources in different time windows (SNR $= 20\,dB$).

As shown in Fig 3, the estimated number of dynamic sources is often equal to the actual number. To see the behavior of the actual and estimated sources, the third and fifth static sources and their estimations during the 20^{th} and 21^{th} time window are zoomed in Fig. 4.

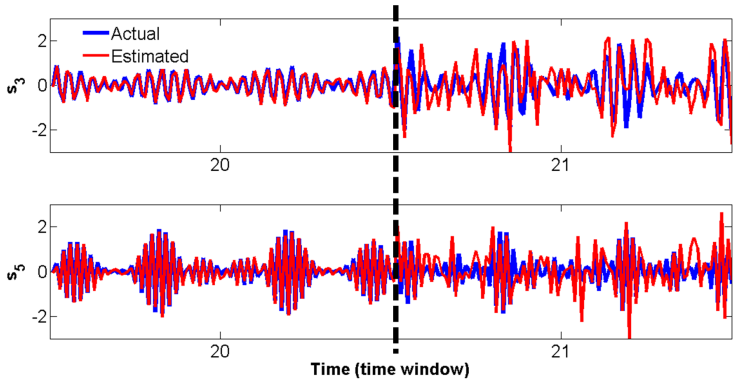

Figure 4: The actual and estimated static sources during the 20^{th} and 21^{th} time window. The vertical dashed line shows the boundary of the time windows.

The normalized squared error ($\|\mathbf{S}^{(k)} - \widehat{\mathbf{S}}^{(k)}\|_F^2 / \|\mathbf{S}^{(k)}\|_F^2$) for the static sources in these time windows are 0.038 and 0.183, respectively. The performance is excellent for the 20^{th} time window where the number of sources is correctly estimated. Conversely, the performance is not very good (as showed both by the high squared error and visual inspection) for the 21^{th} time window where the number of dynamic sources was not estimated correctly (see Fig. 3).

Second Simulation: In this simulation, we repeat the first simulation for different SNR. The values of the criteria introduced in (22) are reported in Table 1.

Table 1: Performance of the proposed method in different SNR.

SNR(dB)	Er_A	Er_S	Er_U	Er_B	Er_r
5	0.146	0.233	0.178	0.127	0.136
10	0.033	0.151	0.097	0.106	0.079
15	0.004	0.089	0.078	0.096	0.041
20	0.002	0.046	0.022	0.037	0.019
25	≤ 0.001	0.006	≤ 0.001	≤ 0.001	0.002

In a specific time window in which the number of dynamic sources was obtained correctly in different SNR, the estimated signals for the first static source are shown in Fig. 5. These results confirm the efficiency of the proposed method in retrieving the model parameters.

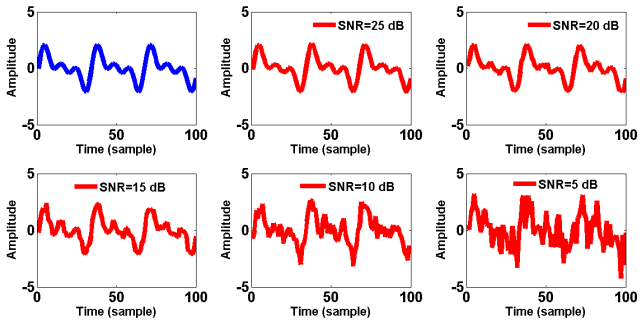

Figure 5: The actual and estimated signals for the first static source in a specific time window in different SNR. The top left figure shows the actual static source.

5.2. Depth Recordings

We recall that the dataset was acquired from four absence epileptic rats using an electrode with $n = 16$ sensors. The recorded data from each rat consisted of few seizures, and each seizure was a train of spike time windows. We apply the proposed method on time windows of a seizure to extract the static and dynamic sources and their structures.

5.2.1. Parameter Extraction (Training Phase)

Since there is no prior information about the number of static sources (m), we apply the proposed method on the seizures for different m and select the one which has suitable biophysiological interpretation. As explained in ($\mathcal{A}1$), the suitable model order must lead to results with intra-rat similarity. In other words, the results should be similar in different seizures of a GAERS rat [18]. Considering this point, the best result is obtained by considering $m = 1$ for all of

the seizures. Since a single static source is sufficient ($m = 1$), the static structure $\mathbf{A} \in \mathbb{R}^{n \times m}$ reduces to a simple vector with $n = 16$ entries. We consider one of the seizures of the first rat which consists of $K = 390$ time windows as the training seizure to show the results.

The obtained static structure (A) and static sources ($s_1^{(k)}(t)$) in different time windows for the training seizure are shown in Fig. 6 (for better representation, we normalized the static sources). It can be observed that the static sources in different time windows are similar, hence, we can consider them as one cluster. The average of this cluster is shown in red. In fact, we can represent all the static sources by only one pattern which is the average of the cluster.

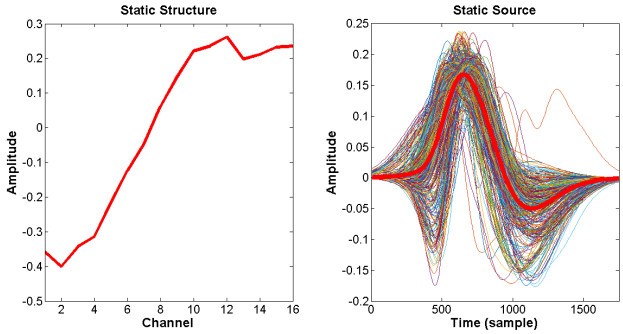

Figure 6: The estimated static structure (left) and the estimated static source in different time windows (right) for the training seizure. To better show the static sources, they are normalized. The average of the static sources is shown in red.

The estimated number of dynamic sources is also equal to one ($r_k = 1$) in all of the time windows of the training seizure. The extracted dynamic structure ($\mathbf{B}^{(k)}$) and source ($u_1^{(k)}(t)$) in different time windows of the training seizure are shown in Fig. 7 (for better representation, the dynamic structures are normalized).

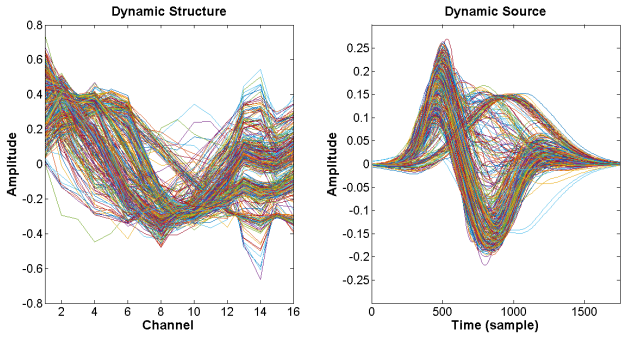

Figure 7: The estimated dynamic structure (left) and the estimated dynamic source in different time windows (right) for the training seizure. To better show the dynamic structures, they are normalized.

By observing the estimated dynamic sources, it can be understood that there are a few kinds of dynamic sources in the training seizure. Therefore, we partition the estimated dynamic sources using *k-means* clustering. The obtained results are shown in the right side of Fig. 8.

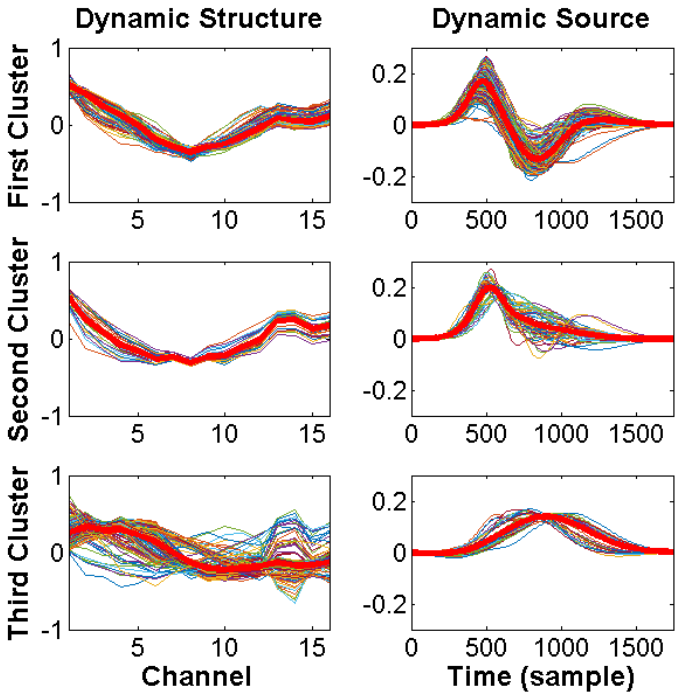

Figure 8: There are three clusters in the dynamic sources. The average of each cluster is shown in red.

As shown in Fig. 8, there are three clusters in the dynamic sources. It should be noted that the suitable criterion for choosing the number of clusters in dynamic sources is that the averages of the clusters corresponding to dynamic sources must have intra-rat similarity, i.e., the results should be similar in different seizures of a specific rat [18]. After determination of the clusters, we also separate their corresponding dynamic structures which are shown in the left side of Fig. 8. The red curves show the averages of the clusters.

Based on the obtained results, we can conclude that there are one static source that we can interpret as modeling the background activity, and three kinds of dynamic sources during the training seizure, which model the different shapes of the spikes and their variability. A linear superposition of the background activity and a dynamic source generates the data in each time window of the training seizure. In fact, this remark answers the first question mentioned in Section 1, and it is illustrated in Fig. 9. We recall that the first question was about the epileptic sources generating the recorded seizures.

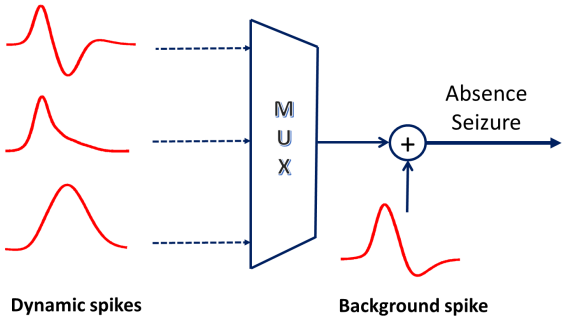

Figure 9: One kind of the dynamic spikes (sources) is added to the background spike (static source) to generate the spike time windows during the training seizure. MUX stands for multiplexer which only allows one dynamic spike to pass in each time window.

Since one kind of dynamic sources participate in the generation of the data in each time windows, we can assign a cluster to each time window. The sequence of clusters for the training seizure is shown in Fig. 10.

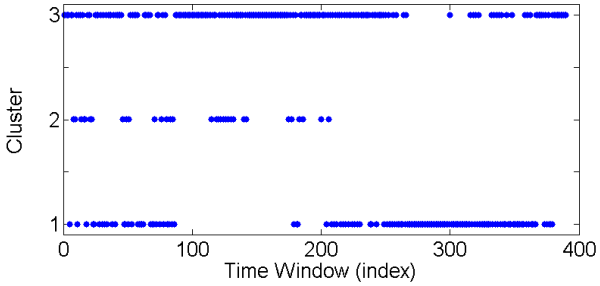

Figure 10: Sequence of clusters for the training seizure.

As shown, all kinds of dynamic sources participate in the generation of the data in the beginning of the training seizure, while in the end of the training seizure, the first and the third dynamic sources just participate in the generation of the data. As mentioned in the beginning of Section 1, the recent theory about the origin of seizures states that in the beginning of seizures, somatosensory cortex drives thalamus, while thereafter, somatosensory cortex and thalamus drive each other until the end of seizures. In fact, a change point exists in the middle of seizures. What we observe in Fig. 10 confirms the existence of such change point during the seizures because one of the sources suddenly disappears in the middle of the seizure. In fact, this paragraph answers the second question mentioned in Section 1. We recall that the second question was about the temporal changes of the recorded seizures.

5.2.2. Results For Other Seizures of The First Rat

We have intra-rat similarity between the results obtained from the seizures of the first rat. This means that the extracted average of the clusters are similar to the results obtained from the training seizure. The sequence of the clusters for one of the seizures which consists of $K = 88$ time windows is shown in Fig. 11. As shown, again, in the end of the seizure, the first and the third dynamic sources only participate in the generation of the seizure.

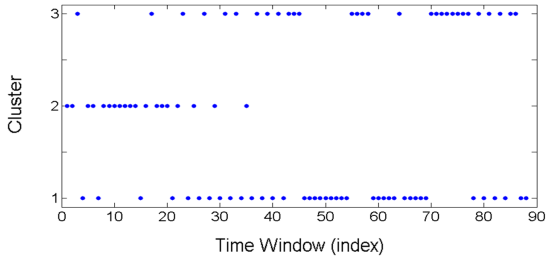

Figure 11: Sequence of clusters for one of the seizures from the first rat which consists of $K = 88$ spike time windows. It is worth mentioning that the time scale differs from Fig. 10 due to the different number of spikes in the seizures.

5.2.3. Results For Other Rats

For other rats, when we extract the model parameters, the interpretable results are again obtained by considering one static source ($m = 1$). The estimated number of dynamic sources is also equal to one ($r_k = 1$) in each time window. Moreover, the same model as Fig. 6 and Fig. 8 can be considered after clustering the sources, i.e., there are three kinds of dynamic sources and a static source. Furthermore, one kind of dynamic sources completely disappears towards the end of the seizures.

For instance, the results obtained from one of the seizures of the second rat are shown in Figs. 12 and 13. Moreover, the sequence of clusters is shown in Fig. 14.

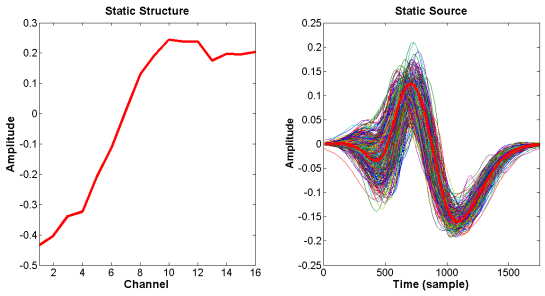

Figure 12: The static structure (left) and sources (right) obtained from one of the absence seizures of the second rat with $K = 560$ time windows.

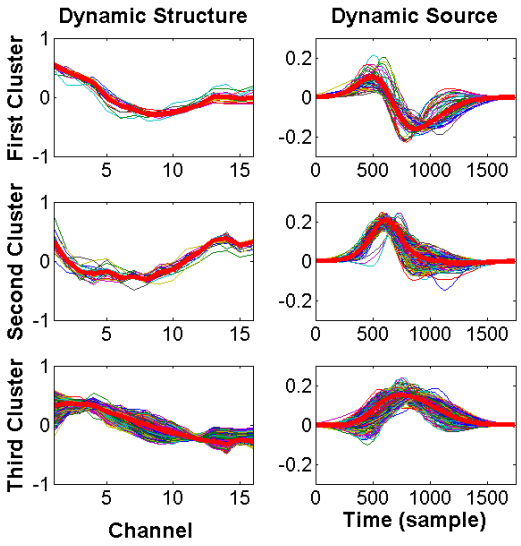

Figure 13: The dynamic structures (left) and sources (right) obtained from one of the absence seizures of the second rat with $K = 560$ time windows.

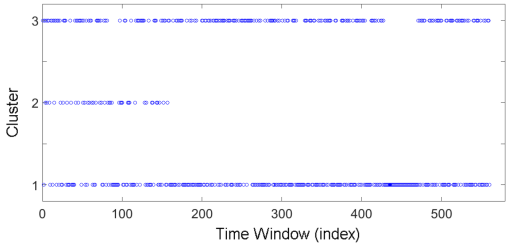

Figure 14: Sequence of clusters for one of the seizures of the second rat which consists of $K = 560$ time windows.

The noticeable point is that the obtained sources in the second rat are different from the ones in the first rat, however, the obtained static structure and averages of clusters for the dynamic structures are similar to ones in the first rat. This means that there is no inter-rat similarity between the obtained sources, while there is inter-rat similarity between the obtained structures. This is quantitatively shown in subsection 5.2.5. Since the structures are related to the arrangement of the sources around the sensors, we can conclude that the origins of the sources are similar in these two rats. Similar results are obtained in other rats. The basic results for one of the other rats are brought in Appendix D.

5.2.4. Adaptation of The Average of Clusters to The Training Seizure

Now, we want to check if the results of clustering (averages of clusters) are adapted to the training seizure or not. For this purpose, we calculate the reconstruction error as explained in the following.

By considering the obtained static structure, the average of the normalized static sources, the average of the normalized dynamic structures, and the average of the dynamic sources respectively as $\mathbf{a}$, $\mathbf{s}$, $\mathbf{b}_j$ $(j = 1, 2, 3)$ and $\mathbf{u}_j$ $(j = 1, 2, 3)$, each time window of the training seizure ($\mathbf{Y}^{(k)}$) and its reconstruction ($\widehat{\mathbf{Y}}^{(k)}$) can be expressed as:

$$\mathbf{Y}^{(k)} = \underbrace{\alpha^{(k)}\mathbf{a}\,\mathbf{s}^T + \sum_{j=1}^{3}\beta_j^{(k)}\mathbf{b}_j\mathbf{u}_j^T}_{\widehat{\mathbf{Y}}^{(k)}} + \mathbf{N}^{(k)} \tag{24}$$

where $\alpha^{(k)}$ and $\beta_j^{(k)}$ are the scaling coefficients because we have normalized the parameters of the model. One of $\beta_j^{(k)}$ $(j = 1, 2, 3)$ is non-zero, and two of them are zero for each time window. Since we already clustered the dynamic sources and structures, the zero entries are known. It can be shown that the MLE solution of $\alpha^{(k)}$ and non-zero $\beta_j^{(k)}$ are as follows:

$$\widehat{\alpha}^{(k)} = Tr\{\mathbf{Y}^{(k)}\,\mathbf{s}\,\mathbf{a}^T\}, \quad \widehat{\beta}_j^{(k)} = Tr\{\mathbf{Y}^{(k)}\mathbf{u}_j\mathbf{b}_j^T\} \tag{25}$$

Now, we can define the reconstruction error as follows:

$$Er_{train} = \frac{1}{K}\sum_{k=1}^{K}\frac{\|\mathbf{Y}^{(k)} - \widehat{\mathbf{Y}}^{(k)}\|_F^2}{\|\mathbf{Y}^{(k)}\|_F^2} \tag{26}$$

This error is equal to 0.03 for the training seizure indicating that the obtained results of clustering are compatible with the training seizure. Now, we want to check if the results of clustering (average of clusters) are also adapted to the other seizures or not.

5.2.5. Cross-Validation (Testing Phase)

We first perform the cross-validation for the seizures of the same rat. We consider one of the seizures as the testing seizure. Then, using the obtained parameters from the training seizure and regarding (24), we estimate the best kind of dynamic source and structure, and scaling coefficients for each time window of the testing seizure. If we again employ the MLE method, we get:

$$\{\widehat{j}, \widehat{\alpha}^{(k)}, \widehat{\beta}_j^{(k)}\} = \underset{j,\alpha^{(k)},\beta_j^{(k)}}{\operatorname{argmin}} \|\mathbf{Y}^{(k)} - \alpha^{(k)}\mathbf{a}\,\mathbf{s}^T - \beta_j^{(k)}\mathbf{b}_j\mathbf{u}_j^T\|_F^2 \tag{27}$$

By determination of the parameters, the reconstructed time window is calculated as follows:

$$\widehat{\mathbf{Y}}^{(k)} = \widehat{\alpha}^{(k)}\mathbf{a}\,\mathbf{s}^T + \widehat{\beta}_{\widehat{j}}^{(k)}\mathbf{b}_{\widehat{j}}\mathbf{u}_{\widehat{j}}^T \tag{28}$$

Now, we calculate the reconstruction error as follows to check the compatibility of the parameters, obtained from the training seizure, with the testing seizure:

$$Er_{test} = \frac{1}{K_{test}} \sum_{k=1}^{K_{test}} \frac{\|\mathbf{Y}^{(k)} - \widehat{\mathbf{Y}}^{(k)}\|_F^2}{\|\mathbf{Y}^{(k)}\|_F^2} \tag{29}$$

where K_{test} shows the number of time windows in the considered testing seizure. We perform the proposed training and testing phase on five seizures of the first rat. The last seizure is the seizure considered in the previous part. The results of the reconstruction are reported in Table 2.

Table 2: Reconstruction error for 5 different seizures of the first rat. The seizures respectively consist of $K_1 = 87$, $K_2 = 94$, $K_3 = 95$, $K_4 = 88$ and $K_5 = 390$ time windows. The diagonal and non-diagonal entries of the table respectively show Er_{train} and Er_{test}.

Training on	Testing on				
seizure	1	2	3	4	5
1	**0.05**	0.11	0.13	0.12	0.09
2	0.07	**0.06**	0.10	0.09	0.08
3	0.08	0.11	**0.06**	0.10	0.09
4	0.10	0.09	0.10	**0.08**	0.10
5	0.09	0.10	0.11	0.12	**0.03**

These results show the intra-rat similarity between seizures, in the sense that the static and dynamic sources and structures trained on one seizure, provide an accurate estimation of signals in other seizures. For other rats, the reconstruction errors have the same order of magnitude as the first rat which show the generality of the results of clustering and proposed model for the recorded seizures.

Since there is no inter-rat similarity between the sources, the aforementioned cross-validation framework between two seizures from two different rats is meaningless. Hence, we calculate the cross correlation coefficient between the results obtained from the two rats. Tables 3 and 4 respectively show the cross correlation coefficient between the obtained structures and sources from the first and second rat.

Table 3: The cross correlation coefficient between the obtained structures from the first and second rat.

First Rat	Second Rat			
	$\mathbf{a}$	$\mathbf{b}_1$	$\mathbf{b}_2$	$\mathbf{b}_3$
$\mathbf{a}$	**0.97**	-0.61	-0.54	-0.72
$\mathbf{b}_1$	-0.58	**0.94**	0.78	0.36
$\mathbf{b}_2$	-0.46	0.77	**0.98**	0.27
$\mathbf{b}_3$	-0.77	0.35	0.32	**0.96**

As reported in Table 3, since the cross correlation coefficients between the structures obtained from two seizures of different rats are close to one, we find

Table 4: The cross correlation coefficient between the obtained sources from the first and second rat.

First Rat	Second Rat			
	$\mathbf{s}$	$\mathbf{u}_1$	$\mathbf{u}_2$	$\mathbf{u}_3$
$\mathbf{s}$	0.83	0.86	0.65	0.53
$\mathbf{u}_1$	0.78	0.81	0.64	0.58
$\mathbf{u}_2$	0.49	0.46	0.88	0.71
$\mathbf{u}_3$	0.63	0.66	0.73	0.79

that the structures in all seizures and all rats are similar, or in other words, they have inter-rat similarity. Since the structures are corresponding to the spatial topography of the sources, we can conclude that the spatial locations of the sources are similar in different rats.

Moreover, as reported in Table 4, since the cross correlation coefficients between the sources obtained from two seizures of different rats are not close to one, we find that the sources do not have inter-rat similarity. Since the sources show the temporal activation functions of their origins, we can conclude that the propagated signals from the origins are not similar in different rats.

We recall that the dataset consists of the data recorded from four GAERS rats, and the data of each rat consist of several seizures. We extracted the sources and their structures from all of the seizures in all of the rats. In summary, the obtained results show that:

1) The structures in all seizures and all rats are similar. In fact, the structures have both intra-rat and inter-rat similarities.

2) The sources in all seizures of a specific rat are similar, but the sources obtained from the seizures of different rats are not similar. In fact, the sources have intra-rat similarity, but they do not have inter-rat similarity.

The results presented in Tables 2, 3, 4 confirm the above conclusions.

In the end of this section, it must be mentioned that the considered model and the proposed method can be adapted to several applications [38, 43, 14] such as radar signals [45, 16], or target tracking in videos [21, 19].

6. Conclusion

In this paper, we analyzed the absence epileptic seizures using depth cortical recordings. The data were recorded from different layers of somatosensory cortex of four absence epileptic rats, and the data of each rat consisted of several seizures. The main goals of the study were 1) retrieving the epileptic activities, or in other words, sources generating the recorded seizures, and 2) finding the dynamics of the recorded seizures. The spike time windows were the most important epileptic events during the recorded seizures. Based on neurophysiological priors and previous contributions, we modeled the spike time windows of each seizure by a linear combination of static and dynamic sources. Then, we proposed an approach to retrieve the static and dynamic sources and their

structures. It is worth mentioning that the structure of the sources represents the contribution of the sources in the generation of data. We extracted the results from all seizures and all rats, and confirmed the generality of the obtained results using a cross-validation framework. The obtained results show that there are a static source and three kinds of dynamic sources during seizures. In fact, there are a background epileptic activity and three dynamic sources which randomly activate with the background activity during the seizures. Moreover, one kind of dynamic sources completely disappear towards the end of the seizures. The obtained results show that the structures have both intra-rat and inter-rat similarities. Hence, we can conclude that the spatial locations of the epileptic sources are similar in different rats. The main difference between the results of different rats is regarding the sources. Although, the sources have intra-rat similarity, but, they do not have inter-rat similarity. In fact, the signals propagated from the epileptic origins are not similar in different rats because the neurons of each rat may have their own specific activation functions. As the future work, it would be interesting if we record data from multiple areas of the cortex using several multisensor electrodes with high spatial resolution. Then, we would have recordings both in different layers of the cortex (column) and in different locations, hence, we can consider both radial and transversal propagations of epileptic events.

7. Acknowledgment

The data used in this study were acquired at Grenoble institute of Neurosciences (GIN) in the team Synchronization and Modulation of Neural Networks in Epilepsy (SyMoNNE) supervised by Dr. A. Depaulis. Also, this work has been partly supported by the European project 2012-ERC-AdG-320684 CHESS.

Bibliography

[1] Akhavan, S., Phlypo, R., Soltanian-Zadeh, H., Kamarei, M., Jutten, C., 2018. Static and dynamic modeling of absence epileptic seizures using depth recordings, in: International Conference on Latent Variable Analysis and Signal Separation, Springer. pp. 534–544.

[2] Akhavan, S., Phlypo, R., Soltanian-Zadeh, H., Studer, F., Depaulis, A., Jutten, C., 2017. Characterizing absence epileptic seizures from depth cortical measurements, in: 2017 25th European Signal Processing Conference (EUSIPCO), pp. 444–448.

[3] Alotaiby, T.N., Alshebeili, S.A., Alshawi, T., Ahmad, I., Abd El-Samie, F.E., 2014. Eeg seizure detection and prediction algorithms: a survey. EURASIP Journal on Advances in Signal Processing 2014, 183.

[4] Amini, L., Jutten, C., Pouyatos, B., Depaulis, A., Roucard, C., 2014. Dynamical analysis of brain seizure activity from eeg signals, in: 2014 22nd European Signal Processing Conference (EUSIPCO), pp. 36–40.

[5] Amor, F., Baillet, S., Navarro, V., Adam, C., Martinerie, J., Le Van Quyen, M., 2009. Cortical Local and Long-range Synchronization Interplay in Human Absence Seizure Initiation. Neuroimage 45, 950–962.

[6] Amor, F., Rudrauf, D., Navarro, V., N'diaye, K., Garnero, L., Martinerie, J., Le Van Quyen, M., 2005. Imaging brain synchrony at high spatiotemporal resolution: application to MEG signals during absence seizures. Signal processing 85, 2101–2111.

[7] Arora, S., Ge, R., Moitra, A., Sachdeva, S., 2015. Provable ica with unknown gaussian noise, and implications for gaussian mixtures and autoencoders. Algorithmica 72, 215–236.

[8] Avoli, M., 2012. A brief history on the oscillating roles of thalamus and cortex in absence seizures. Epilepsia 53, 779–789.

[9] Belloni, A., Chernozhukov, V., Wang, L., 2011. Square-root lasso: pivotal recovery of sparse signals via conic programming. Biometrika 98, 791.

[10] Cabasson, A., Meste, O., 2008. Time delay estimation: A new insight into the woody's method. IEEE Signal Processing Letters 15, 573–576.

[11] Candes, E.J., Plan, Y., 2010. Matrix completion with noise. Proceedings of the IEEE 98, 925–936.

[12] Caraballo, R.H., Fontana, E., Darra, F., Bongiorni, L., Fiorini, E., Cersosimo, R., Fejerman, N., Bernardina, B.D., 2008. Childhood absence epilepsy and electroencephalographic focal abnormalities with or without clinical manifestations. Seizure 17, 617 – 624.

[13] Cardoso, J.F., Souloumiac, A., 1993. Blind beamforming for non-gaussian signals. IEEE Proceedings F - Radar and Signal Processing 140, 362–370.

[14] Chandrasekhar, A., Natarajan, K., Yavarimanesh, M., Mukkamala, R., 2018. An iphone application for blood pressure monitoring via the oscillometric finger pressing method. Scientific reports 8, 13136.

[15] Comon, P., Jutten, C., 2010. Handbook of Blind Source Separation: Independent Component Analysis and Applications. Elsevier.

[16] Dai, B., Wang, T., Wu, J., Bao, Z., 2015. Adaptively iterative weighting covariance matrix estimation for airborne radar clutter suppression. Signal Processing 106, 282–293.

[17] Das, A., Folland, R., Stocks, N.G., Hines, E.L., 2006. Stimulus reconstruction from neural spike trains: Are conventional filters suitable for both periodic and aperiodic stimuli? Signal processing 86, 1720–1727.

[18] Depaulis, A., David, O., Charpier, S., 2016. The genetic absence epilepsy rat from strasbourg as a model to decipher the neuronal and network mechanisms of generalized idiopathic epilepsies. Journal of neuroscience methods 260, 159–174.

[19] Du, B., Sun, Y., Wu, C., Zhang, L., Zhang, L., 2017. Real-time tracking based on weighted compressive tracking and a cognitive memory model. Signal Processing 139, 173–181.

[20] Einevoll, G.T., Kayser, C., Logothetis, N.K., Panzeri, S., 2013. Modelling and analysis of local field potentials for studying the function of cortical circuits. Nature Reviews Neuroscience 14, 770–785.

[21] Hu, M., Liu, Z., Zhang, J., Zhang, G., 2017. Robust object tracking via multi-cue fusion. Signal Processing 139, 86–95.

[22] Kelley, C., 1999. Iterative Methods for Optimization. Frontiers in Applied Mathematics, Society for Industrial and Applied Mathematics.

[23] Koochakzadeh, A., Malek-Mohammadi, M., Babaie-Zadeh, M., Skoglund, M., 2015. Multi-antenna assisted spectrum sensing in spatially correlated noise environments. Signal Processing 108, 69–76.

[24] Li, X., Ouyang, G., Richards, D.A., 2007. Predictability analysis of absence seizures with permutation entropy. Epilepsy research 77, 70–74.

[25] van Luijtelaar, G., Lüttjohann, A., Makarov, V.V., Maksimenko, V.A., Koronovskii, A.A., Hramov, A.E., 2016. Methods of automated absence seizure detection, interference by stimulation, and possibilities for prediction in genetic absence models. Journal of neuroscience methods 260, 144–158.

[26] Malek-Mohammadi, M., Babaie-Zadeh, M., Skoglund, M., 2015. Performance guarantees for schatten-p quasi-norm minimization in recovery of low-rank matrices. Signal Processing 114, 225–230.

[27] Marten, F., Rodrigues, S., Suffczynski, P., Richardson, M.P., Terry, J.R., 2009. Derivation and analysis of an ordinary differential equation mean-field model for studying clinically recorded epilepsy dynamics. Phys. Rev. E 79, 021911.

[28] Mazzoni, A., Logothetis, N.K., Panzeri, S., 2013. Information content of local field potentials , 411–430.

[29] Meeren, H.K.M., Pijn, J.P.M., Coenen, A.M.L., Lopes Da Silva, O.H., 2002. Cortical Focus Drives Widespread Corticothalamic Networks During Spontaneous Absence Seizures in Rats. J. Neurosci 22, 1480–1495.

[30] Moeller, F., LeVan, P., Muhle, H., Stephani, U., Dubeau, F., Siniatchkin, M., Gotman, J., 2010. Dynamic analysis of absence seizures in humans: all the same but all different. Neuropediatrics 41, V1287.

[31] Moeller, F., Siniatchkin, M., LeVan, P., Stephani, U., Dubeau, F., Gotman, J., 2009. Dynamic analysis of absence seizures in humans–an eeg fmri study. Neuroimage , 91.

[32] Panayiotopoulos, C.P., 2008. Typical absence seizures and related epileptic syndromes: Assessment of current state and directions for future research. Epilepsia 49, 2131–2139.

[33] Panayiotopoulos, C.P., 2010. A Clinical Guide to Epileptic Syndromes and their Treatment. Springer London.

[34] Polack, P.O., Guillemain, I., Hu, E., Deransart, C., Depaulis, A., Charpier, S., 2007. Deep Layer Somatosensory Cortical Neurons Initiate Spike-and-Wave Discharges in a Genetic Model of Absence Seizures. The Journal of Neuroscience 27, 6590–6599.

[35] Quiroga, R.Q., Nadasdy, Z., Ben-Shaul, Y., 2004. Unsupervised Spike Detection And Sorting With Wavelets And Superparamagnetic Clustering. Neural Comput 16, 1661–1687.

[36] Recht, B., Fazel, M., Parrilo, P.A., 2010. Guaranteed minimum-rank solutions of linear matrix equations via nuclear norm minimization. SIAM Review 52, 471–501.

[37] Seth, A.K., Barrett, A.B., Barnett, L., 2015. Granger causality analysis in neuroscience and neuroimaging. Journal of Neuroscience 35, 3293–3297.

[38] Shirzadian Gilan, M., Yavari Manesh, M., Mohammadi, A., 2016. Level crossing rate and average fade duration of amplify and forward relay channels with cochannel interference, in: European Wireless 2016; 22th European Wireless Conference, pp. 1–5.

[39] Steriade, M., 2003. Neuronal Substrates of Sleep and Epilepsy. Cambridge University Press.

[40] Toh, K.C., Todd, M.J., Tütüncü, R.H., 1999. SDPT3 — a matlab software package for semidefinite programming, version 1.3. Optimization Methods and Software 11, 545–581.

[41] Vlachos, I., Krishnan, B., Treiman, D.M., Tsakalis, K., Kugiumtzis, D., Iasemidis, L.D., 2017. The concept of effective inflow: Application to interictal localization of the epileptogenic focus from ieeg. IEEE Transactions on Biomedical Engineering 64, 2241–2252.

[42] Wu, C., Xiang, J., Sun, J., Huang, S., Tang, L., Miao, A., Zhou, Y., Chen, Q., Hu, Z., Wang, X., 2017. Quantify neuromagnetic network changes from pre-ictal to ictal activities in absence seizures. Neuroscience 357, 134–144.

[43] Yavari Manesh, M., Olfat, A., 2017. Sigmoid function detector in the presence of heavy-tailed noise for multiple antenna cognitive radio networks, in: 2017 IEEE International Conference on Communications (ICC), pp. 1–5.

[44] Yeredor, A., 2002. Non-orthogonal joint diagonalization in the least-squares sense with application in blind source separation. IEEE Transactions on Signal Processing 50, 1545–1553.

[45] Zhu, J., Wang, X., Huang, X., Suvorova, S., Moran, B., 2018. Detection of moving targets in sea clutter using complementary waveforms. Signal Processing 146, 15–21.

Appendices

A. Extraction of The static structure

By assuming $\mathbf{Z}^{(k)} = \mathbf{R}_y^{(k)} - \mathbf{R}_B^{(k)}$, we get:

$$\begin{aligned} \widehat{\mathbf{A}} = \underset{\mathbf{A}}{\operatorname{argmin}} \sum_{k=1}^{K} \|\mathbf{Z}^{(k)} - \mathbf{A}\mathbf{\Lambda}_s^{(k)}\mathbf{A}^T\|_F^2 \\ s.t. \quad diag(\mathbf{A}^T\mathbf{A}) = \mathbf{I} \end{aligned} \tag{30}$$

We solve this optimization problem using gradient projection (GP) method. We iteratively perform the following steps (gradient and projection) until convergence of $\mathbf{A}$.

Gradient Step: In the gradient step, we use the Newton method to speed up the convergence. The gradient and Hessian of the objective function with respect to $\mathbf{A}$ is calculated as follows:

$$\begin{aligned} \mathbf{G} &= \sum_{k=1}^{K} 4\mathbf{A}\mathbf{\Lambda}_s^{(k)}\mathbf{A}^T\mathbf{A}\mathbf{\Lambda}_s^{(k)} - 2\mathbf{Z}^{(k)}\mathbf{A}\mathbf{\Lambda}_s^{(k)} \\ \mathbf{H} &= \sum_{k=1}^{K} 4(\mathbf{\Lambda}_s^{(k)}\mathbf{A}^T\mathbf{A}\mathbf{\Lambda}_s^{(k)} \otimes \mathbf{I}) + 4(\mathbf{\Lambda}_s^{(k)}\mathbf{A}^T \otimes \mathbf{A}\mathbf{\Lambda}_s^{(k)})\mathbf{\Pi} \\ &\quad +4(\mathbf{\Lambda}_s^{(k)} \otimes \mathbf{A}\mathbf{\Lambda}_s^{(k)}\mathbf{A}^T) - 2(\mathbf{\Lambda}_s^{(k)} \otimes \mathbf{Z}^{(k)}) \end{aligned} \tag{31}$$

where $\otimes$ denotes the Kronecker product, $\mathbf{I} \in \mathbb{R}^{n \times n}$ is the identity matrix, and $\mathbf{\Pi} \in \mathbb{R}^{n^2 \times n^2}$ is the permutation matrix which provides the following equality:

$$vec(\mathbf{A}^T) = \mathbf{\Pi}\, vec(\mathbf{A}) \tag{32}$$

where $vec(\mathbf{A})$ denotes a long vector obtained by stacking the columns of $\mathbf{A}$. Hence, by considering $\mathbf{a} = vec(\mathbf{A})$ and $\mathbf{g} = vec(\mathbf{G})$, we perform the following iteration in this step:

$$\mathbf{a} \leftarrow \mathbf{a} - \mathbf{H}^{-1}g$$

Then, we reshape $\mathbf{a}$ to construct its matricization form.

Projection (Normalization) Step: In this step, each column of $\mathbf{A}$ is normalized.

B. Extracting auto-correlation matrix of static sources

By assuming $\mathbf{Z}^{(k)} = \mathbf{R}_y^{(k)} - \mathbf{R}_B^{(k)}$, we get:

$$\begin{aligned} \widehat{\mathbf{\Lambda}}_s^{(k)} &= \underset{\mathbf{\Lambda}_s^{(k)}}{\operatorname{argmin}} \|\mathbf{Z}^{(k)} - \mathbf{A}\mathbf{\Lambda}_s^{(k)}\mathbf{A}^T\|_F^2 \\ s.t. \quad & \mathbf{\Lambda}_s^{(k)} = diag(\mathbf{\Lambda}_s^{(k)}), \quad \mathbf{\Lambda}_s^{(k)} \succeq 0 \end{aligned} \tag{33}$$

We consider the vectorized form of the proposed objective function as:

$$\widehat{\lambda}_s^{(k)} = \underset{\lambda_s^{(k)}}{\operatorname{argmin}} \|\mathbf{z}^{(k)} - \mathbf{Q}\lambda_s^{(k)}\|_2^2 \tag{34}$$

where $\lambda_s^{(k)} = vec(\mathbf{\Lambda}_s^{(k)}) \in \mathbb{R}^{m^2}$, $\mathbf{z}_s^{(k)} = vec(\mathbf{Z}^{(k)}) \in \mathbb{R}^{n^2}$, $\mathbf{Q} = \mathbf{A} \otimes \mathbf{A} \in \mathbb{R}^{n^2 \times m^2}$, and $\otimes$ denotes the Kronecker product. Since we know that $\lambda_s^{(k)}$ just has n non-zero entries, we consider the non-zero entries of $\lambda_s^{(k)}$ in $\lambda_{s_1}^{(k)} \in \mathbb{R}^m$, and also, the columns of $\mathbf{Q}$ corresponding to the non-zero entries of $\lambda_s^{(k)}$ in $\mathbf{Q}_1 \in \mathbb{R}^{n^2 \times m}$. Hence, (33) can be expressed as:

$$\begin{aligned} \widehat{\lambda}_{s_1}^{(k)} &= \underset{\lambda_{s_1}^{(k)}}{\operatorname{argmin}} \|\mathbf{z}^{(k)} - \mathbf{Q}_1\lambda_{s_1}^{(k)}\|_2^2 \\ & s.t. \quad \lambda_{s_1}^{(k)} \geq 0 \end{aligned} \tag{35}$$

where $\lambda_{s_1}^{(k)} \geq 0$ means each entry of $\lambda_{s_1}^{(k)}$ must be non-negative. This optimization problem is a non-negative least square (NNLS) problem. There are many toolboxes that can be employed to solve this problem very fast (e.g., *nnls* function in MATLAB).

C. Extraction of $\mathbf{R}_B^{(k)}$

By assuming $\mathbf{Z}^{(k)} = \mathbf{R}_y^{(k)} - \mathbf{A}\mathbf{\Lambda}_s^{(k)}\mathbf{A}^T$, we get:

$$\begin{aligned} \widehat{\mathbf{R}}_B^{(k)} &= \underset{\mathbf{R}_B^{(k)}}{\operatorname{argmin}} \|\mathbf{Z}^{(k)} - \mathbf{R}_B^{(k)}\|_F + \lambda^{(k)} \ Tr(\mathbf{R}_B^{(k)}) \\ & s.t. \quad \mathbf{R}_B^{(k)} \succeq 0 \end{aligned} \tag{36}$$

If we consider $\mathbf{r} = vec(\mathbf{Z}^{(k)} - \mathbf{R}_B^{(k)}) \in \mathbb{R}^{n^2}$, we can write (36) as:

$$\begin{aligned} \widehat{\mathbf{R}}_B^{(k)} &= \underset{t, \mathbf{R}_B^{(k)}}{\operatorname{argmin}} \ t + \lambda^{(k)} \ Tr(\mathbf{R}_B^{(k)}) \\ s.t. \quad & \mathbf{R}_B^{(k)} \succeq 0, \quad \sqrt{\mathbf{r}^T\mathbf{r}} \leq t \end{aligned} \tag{37}$$

Moreover, using a Schur complement argument, the constraint $\sqrt{\mathbf{r}^T\mathbf{r}} \leq t$ is equivalent to:

$$\begin{bmatrix} t\mathbf{I} & \mathbf{r} \\ \mathbf{r}^T & t \end{bmatrix} \succeq 0 \tag{38}$$

where $\mathbf{I} \in \mathbb{R}^{n^2 \times n^2}$ is the identity matrix. Hence, we can express (36) as the following semidefinite programming (SDP) problem:

$$\begin{aligned} \widehat{\mathbf{R}}_B^{(k)} = \underset{t, \mathbf{R}_B^{(k)}}{\operatorname{argmin}} \; & t + \lambda^{(k)} \operatorname{Tr}(\mathbf{R}_B^{(k)}) \\ s.t. \quad & \begin{bmatrix} \mathbf{R}_B^{(k)} & 0 & 0 \\ 0 & t\mathbf{I} & \mathbf{r} \\ 0 & \mathbf{r}^T & t \end{bmatrix} \succeq 0 \end{aligned} \tag{39}$$

This kind of problems can be solved using well known solvers like sdpt3 and cvx [40]. Regarding the penalty term, we can consider the proposed value in square-root LASSO problem[9] because the two problems are the same. The penalty term is independent of the noise variance and obtained as follows according to [9]:

$$\lambda^{(k)} = \frac{c}{n} \phi^{-1}(1 - \frac{\alpha}{2n^2}) \tag{40}$$

where $c > 1$ is a constant, ϕ is the cumulative distribution function (CDF) of a zero-mean and unit variance Gaussian variable, and $1 - \alpha$ is the probability of detection.

D. Results for Other Rats

The results obtained from one of the seizures of the third rat which consists of $K = 253$ time windows are shown in Figs. 15 and 16. Moreover, the sequence of clusters is shown in Fig. 17.

As discussed before and observed in Figs. 15 and 16, the structures have both intra-rat and inter-rat similarities, while the sources just have intra-rat similarity. Moreover, as shown in Fig. 17, one of the dynamic sources disappear towards the end of the seizures.

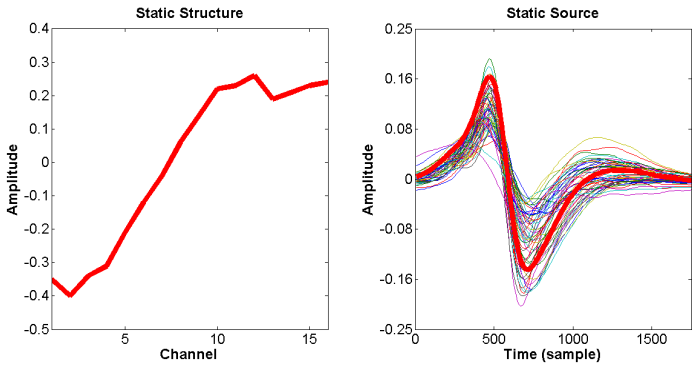

Figure 15: The static structure (left) and sources (right) obtained from one of the absence seizures of the third rat with $K = 253$ time windows.

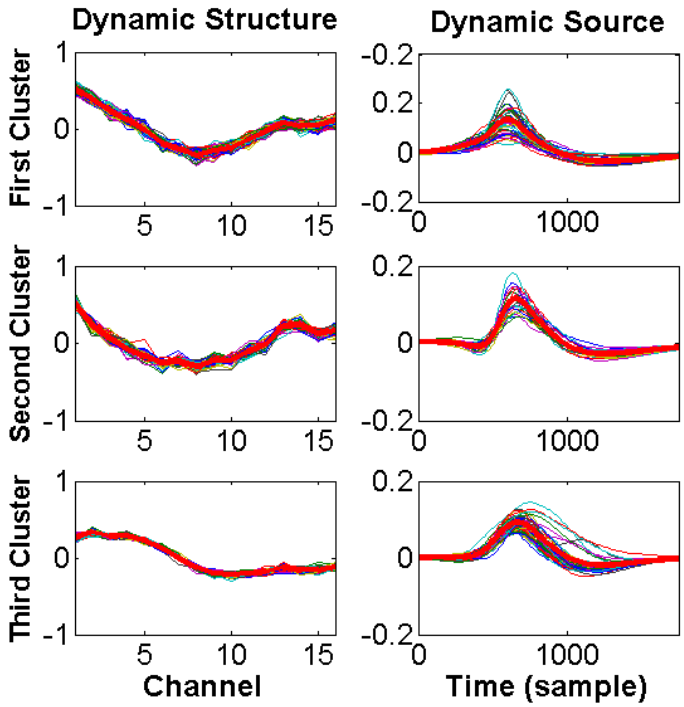

Figure 16: The dynamic structures (left) and sources (right) obtained from one of the absence seizures of the third rat with $K = 253$ time windows.

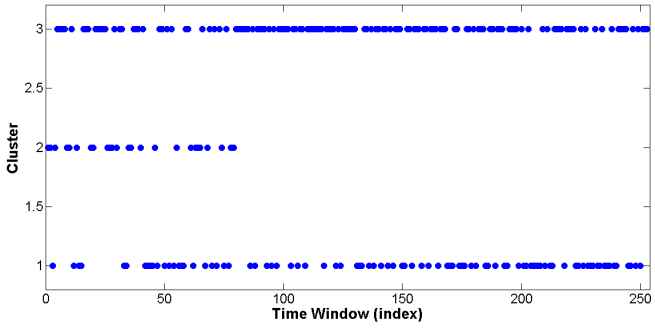

Figure 17: Sequence of clusters for one of the seizures of the third rat which consists of $K = 253$ time windows.